Supporting Information

The surface energy modulation of van der Waals interface in atomically thin semiconductor

Dae Young Park[1,#], Hyeong Chan Suh[1,#], Seungho Bang[1], Juchan Lee[1], Jaekak Yoo[2,3], Hayoung Ko[2], Soo Ho Choi[2], Ki Kang Kim[2],Seung Mi Lee[3], Seong Chu Lim[2], Tschang-Uh Nahm[1], and Mun Seok Jeong[1,]*

[1]Department of Physics, Hanyang University, Seoul 04763, Republic of Korea

[2]Department of Energy Science, Sungkyunkwan University, Suwon 16419, Republic of Korea

[3]Korea Research Institute of Standards and Science, Daejeon 34113, Republic of Korea

* Address correspondence to mjeong@hanyang.ac.kr (M.S.J.)

This supporting information includes:

Figure S1. The morphology of a) $MoSe_2$, b) WS_2, and c) WSe_2 on S10 (top) and SiO_2 (bottom) surfaces.
Figure S2. The XPS spectra of the 1s orbital of Carbon, Fluorine, and Oxygen for a) SiO_2 and b) S10, respectively.
Figure S3. Ultraviolet photoelectron spectroscopy of TMDCs on SiO_2 and S10, respectively.
Figure S4. The atomic charge distribution of TMDCs/S10 heterostructure through Mulliken analysis.
Figure S5. The electrical transport of pristine MoS_2 devices.
Figure S6. The electrical transport of pristine MoS_2/S10 devices.
Figure S7. The comparison of electrical properties for the devices of TMDCs monolayer on S10 and SiO_2, respectively.

Table S1. Electronegativity, bonding character, and dipole moment of TMDCs.
Table S2. Biding energy of transition metal and chalcogenide in TMDCs on the SiO_2 and S10.
Table S3. The changes of dipole moment depending on S10.
Table S4. The comparison of field effect mobility and subthreshold swing in TMDCs monolayer on SiO_2 and S10.

Supporting Note 1
Supporting Note 2
Supporting Note 3

References

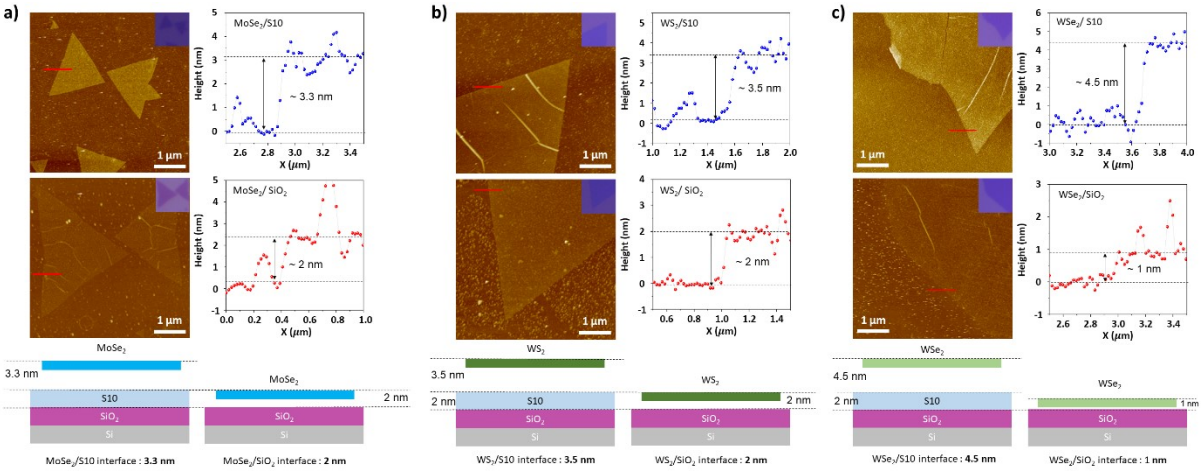

Figure S1. The morphology of a) $MoSe_2$, b) WS_2, and c) WSe_2 on S10 (top) and SiO_2 (bottom) surfaces.

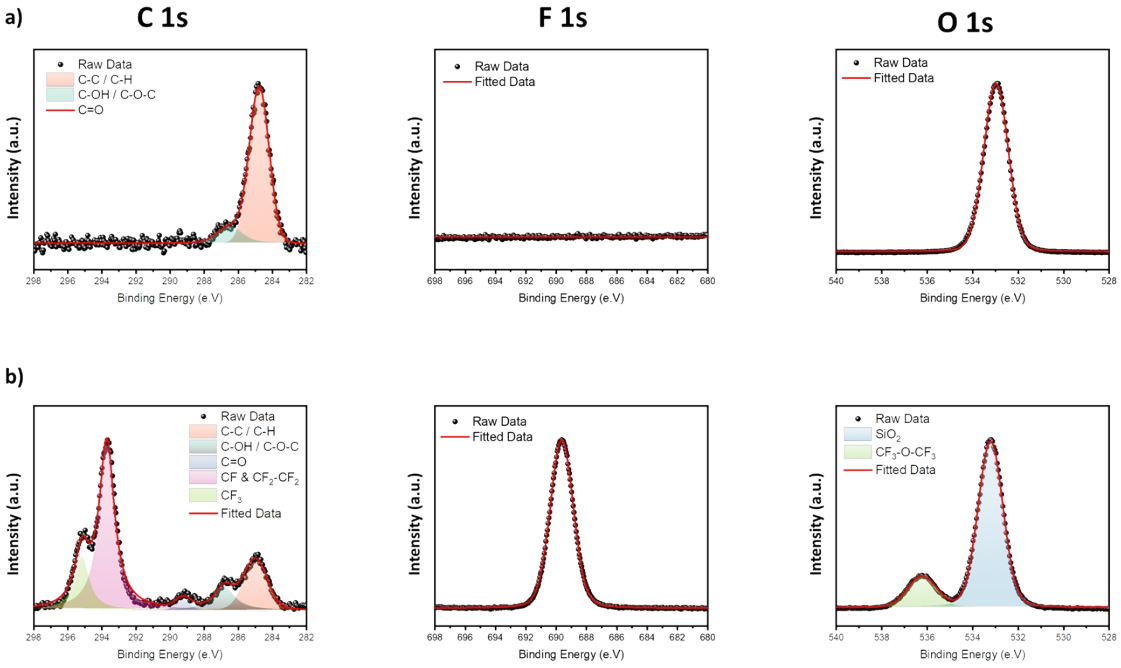

Figure S2. The XPS spectra of the 1s orbital of Carbon, Fluorine, and Oxygen for a) SiO_2 and b) S10, respectively.

Table S1. Electronegativity, bonding character, and dipole moment of TMDCs.

Atom	Electronegativity (χ)	TMDCs	Ionic bonding (%)	Covalent bonding (%)	Bond length (Å)	Dipole moment (Debye)
Mo	2.16	MoS_2	4.31	95.69	2.42	0.50
W	2.36	$MoSe_2$	3.73	96.27	2.49	0.45
S	2.58	WS_2	1.20	98.80	2.40	0.14
Se	2.55	WSe_2	0.90	99.10	2.49	0.11

Table S2. Biding energy of transition metal and chalcogenide in TMDCs on the SiO_2 and S10.

MoS_2				
Substrate	Binding Energy (eV)			
	Mo $3d_{5/2}$	Mo $3d_{3/2}$	S $2p_{3/2}$	S $2p_{1/2}$
SiO_2	229.58	232.73	162.38	163.56
S10	230.03	233.17	162.84	164.01
Shift	0.45	0.44	0.46	0.45

WS_2					
Substrate	Binding Energy (eV)				
	W $4f_{7/2}$	W $4f_{5/2}$	W $5p_{3/2}$	S $2p_{3/2}$	S $2p_{1/2}$
SiO_2	33.43	35.59	38.95	163.11	164.31
S10	32.74	34.74	37.48	162.22	163.41
Shift	-0.69	-0.85	-1.47	-0.89	-0.9

$MoSe_2$				
Substrate	Binding Energy (eV)			
	Mo $3d_{5/2}$	Mo $3d_{3/2}$	Se $3d_{5/2}$	Se $3d_{3/2}$
SiO_2	229.03	232.18	54.43	55.3
S10	229.11	232.23	54.53	55.37
Shift	0.08	0.05	0.1	0.07

WSe_2					
Substrate	Binding Energy (eV)				
	W $4f_{7/2}$	W $4f_{5/2}$	W $5p_{3/2}$	Se $3d_{5/2}$	Se $3d_{3/2}$
SiO_2	32.58	34.75	38.05	54.85	55.68
S10	32.02	34.19	37.66	54.28	55.12
Shift	-0.56	-0.56	-0.39	-0.57	-0.56

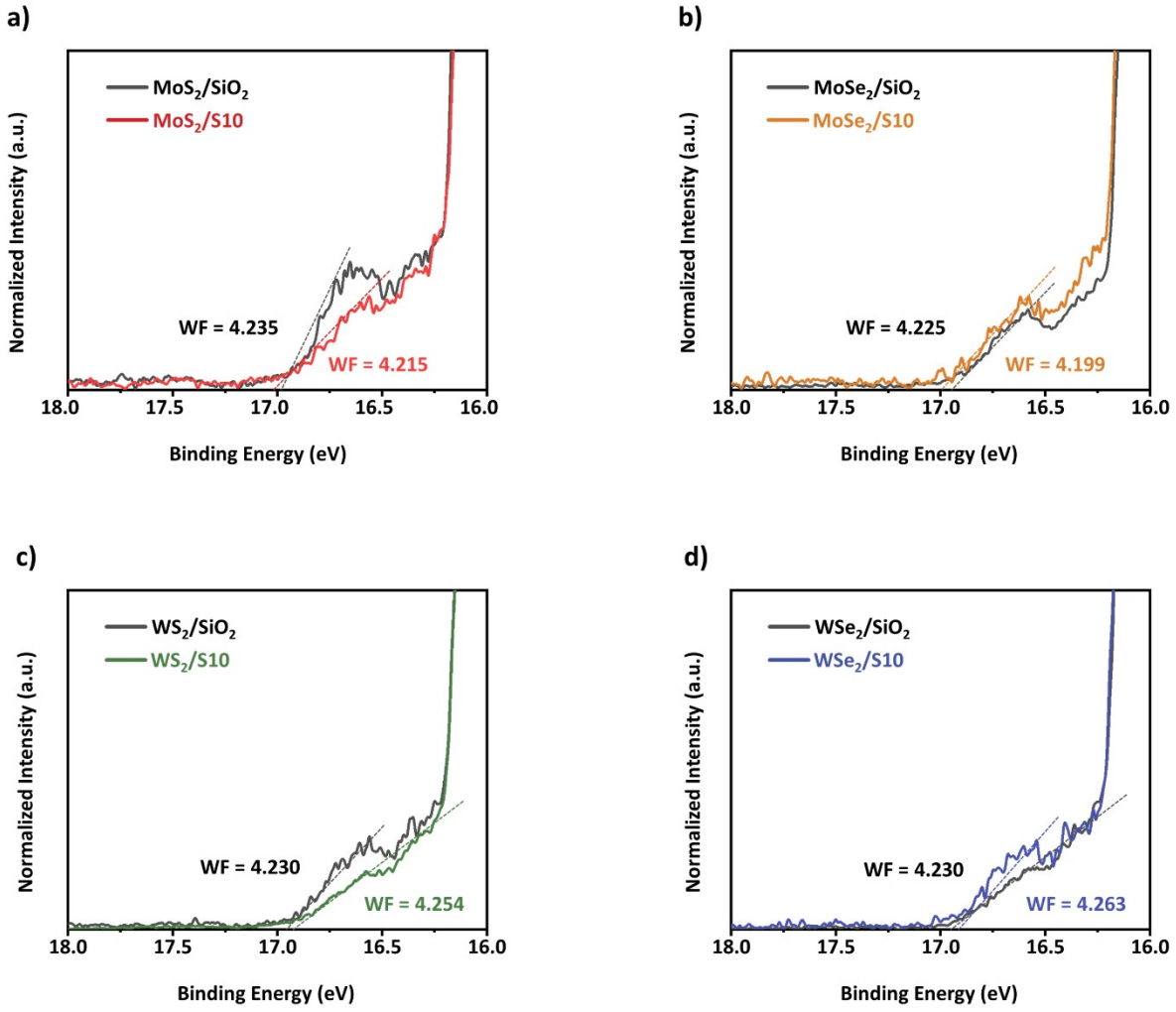

Figure S3. Ultraviolet photoelectron spectroscopy of TMDCs on SiO2 and S10, respectively. a) MoS_2, b) $MoSe_2$, c) WS_2, and d) WSe_2.

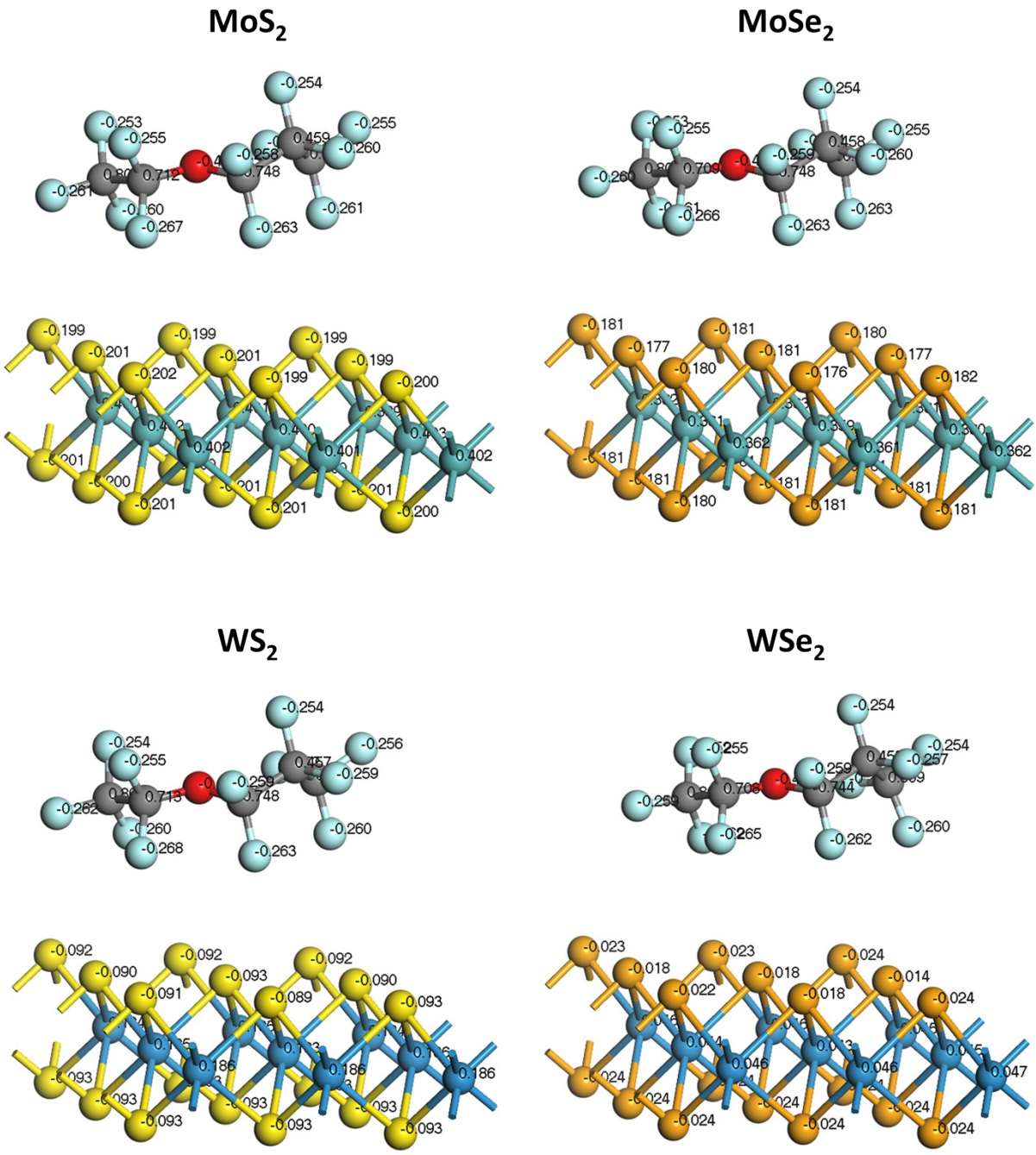

Figure S4. The atomic charge distribution of TMDCs/S10 heterostructure through Mulliken analysis.

Table S3. The changes of dipole moment depending on S10.

TMDCs	Bond length (Å)	Intrinsic Dipole moment (Debye)	Induced Dipole moment with S10 (Debye)
MoS_2	2.42	0.50	0.93
$MoSe_2$	2.49	0.45	0.78
WS_2	2.40	0.14	0.19
WSe_2	2.49	0.11	0.01

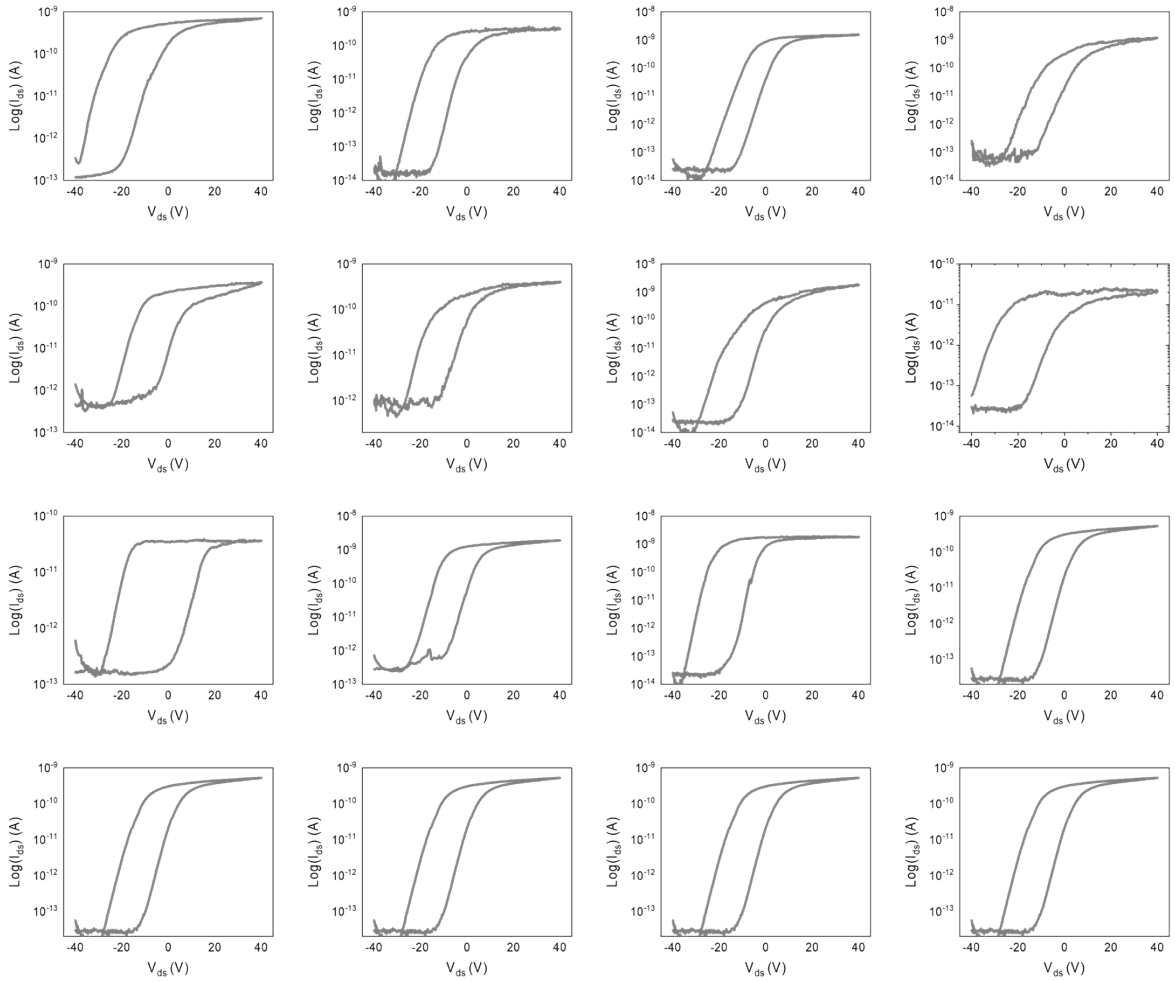

Figure S5. The electrical transport of pristine MoS_2 devices.

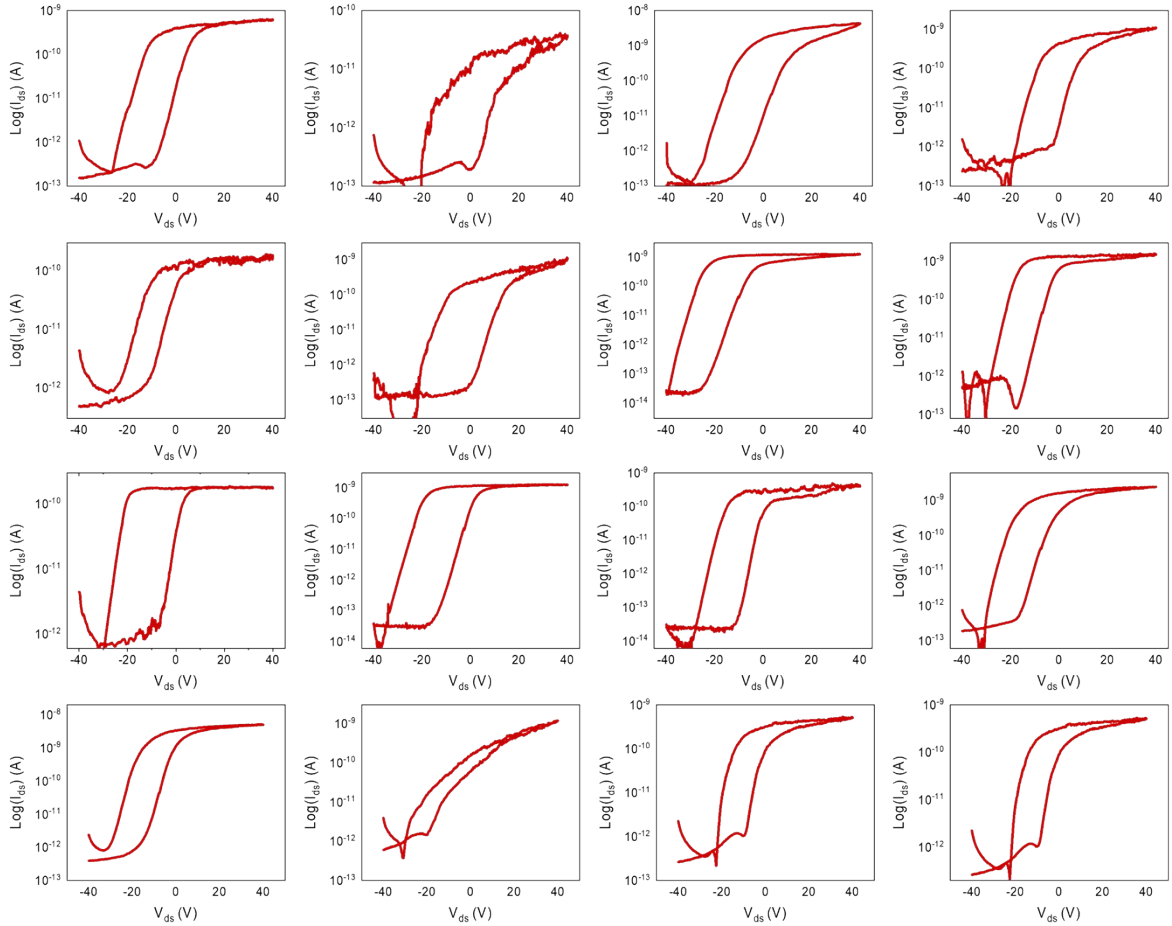

Figure S6. The electrical transport of pristine MoS_2/S10 devices.

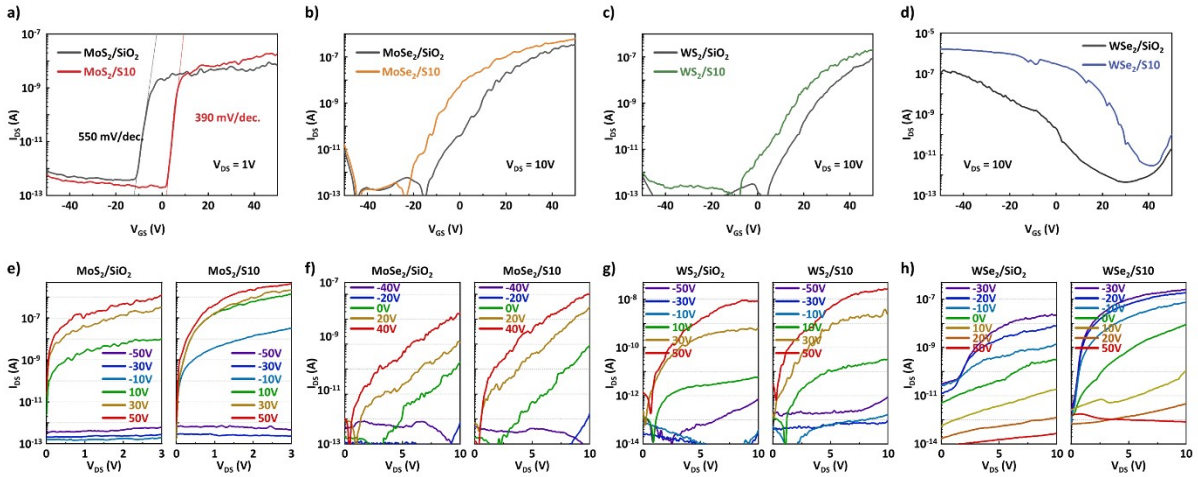

Figure S7. The comparison of electrical properties for the devices of TMDCs monolayer on S10 and SiO_2, respectively. The transfer curves of a) MoS_2, b) $MoSe_2$, c) WS_2, d) WSe_2 and the output curves of e) MoS_2, f) $MoSe_2$, g) WS_2, h) WSe_2 are presented, respectively.

Table S4. The comparison of field effect mobility and subthreshold swing in TMDCs monolayer on SiO_2 and S10.

TMDCs	**MoS_2**		**$MoSe_2$**		**WS_2**		**WSe_2**	
	SiO_2	S10	SiO_2	S10	SiO_2	S10	SiO_2	S10
Field effect mobility (cm^2/Vs)	0.042	0.082	0.123	0.251	0.089	0.185	0.140	0.301
SS (mV/dec.)	550	390	2,790	1,720	6,100	3,190	3,690	1,560

Supporting Note 1

To determine the electron populations of transition metal dichalcogenides (TMDCs) when perfluoropolyether (PFPE) approaches, we performed quantum mechanical calculations using DMOL3 code as implemented in the BIOVIA Materials Studio platform. The double numeric atomic orbitals with polarization for the basis sets, and all electrons, with a relativistic effect considered for the core parts, were used during calculation. The exchange-correlation functionals with generalized gradient approximation[1], and the *k*-points samplings by Monkhorst-Pack grid with equidistance of 0.02 $Å^{-1}$ were chosen. The lattice constants of optimized bulk TMDCs using calculational parameters listed above follows: $a = b = 3.19$ Å and $c = 14.88$ Å for MoS_2, $a = b = 3.33$ Å and $c = 15.45$ Å for $MoSe_2$, $a = b = 3.19$ Å and $c = 14.20$ Å for WS_2, and $a = b = 3.30$ Å and $c = 15.07$ Å for WSe_2. The optimized structures are well matched with previous results: $a = b = 3.15$ Å and $c = 12.3$ Å for MoS_2, $a = b = 3.3$ Å and $c = 13.0$ Å for $MoSe_2$, $a = b = 3.15$ Å and $c = 12.32$ Å for WS_2, and $a = b = 3.29$ Å, and $c = 12.98$ Å for WSe_2.

From the optimized geometry, we generated (3×3) supercell and cleaved the (0 0 1) surface to consider the population differences of surface. After that, we applied 60 Å of vacuum slab to exclude interlayer interaction. The monomer of PFPE was used to accelerate the simulation. To consider the actual experimental conditions, we first modeled PFPE on the TMDCs surface with a 1 Å distance. As a result of geometry optimization, the distance between PFPE and TMDCs surface became 3 Å naturally due to Coulomb interaction matching to AFM measurement. After that, the contributions to the atomic charge from each atomic orbital on each atom were calculated using Mulliken-analysis method.

Supporting Note 2

The calculation for the changes of dipole moment on S10 was conducted using the equation shown below:

$\mu = q \cdot r$

u, q, r are dipole moment, separated charge, and bond length of transition metal and chalcogen, respectively. The separated charge of TMDs by S10 was calculated by the equation, $q = ed_c$, (e: a charge of electron, d_c: atomic charge distribution in figure S3).

Supporting Note 3

The field-effect mobility (μ_{FE}) for each TMDC were calculated using the following equations:

$$\mu_{FE} = g_m \frac{L}{W C_{ox} V_{DS}} \frac{1}{}$$

where, g_m is the maximum back-gated transconductance. L and W are the length (8 μm) and width (25 μm) of the channel, respectively. C_{OX} (=$\varepsilon_0 \cdot \varepsilon_r$/d; ε_r=3.9) represents the back-gate capacitance of SiO_2 (300 nm). V_{DS} is the drain-source voltage.

The subthreshold swing (SS) of devices were calculated using the equation shown below:

$$SS = \left(\frac{d(\log_{10} I_{DS})}{dV_{GS}} \right)^{-1}$$

References

(1) J. P. Perdew, J.P.; Burke, K.; Ernzerhof, M., Generalized Gradient Approximation Made Simple: *Phys. Rev. Lett.* **1996**, 77, 3865.

(2) Voß, D.; Krüger, P.; Mazur, A.; Pollmann, J. Atomic and Electronic Structure of from Ab Initio Theory: Bulk Crystal and Thin Film Systems. *Phys. Rev. B: Condens. Matter Mater. Phys.* **1999**, *60* (20), 14311.

(3) Roy, A.; Movva, H. C. P.; Satpati, B.; Kim, K. Structural and Electrical Properties of $MoTe_2$ and $MoSe_2$ Grown by Molecular Beam Epitaxy. *ACS Appl. Mater. Interfaces* **2016**, *8* (11), 7396–7402.

(4) Molina-Sánchez, A.; Wirtz, L. Phonons in Single-Layer and Few-Layer MoS_2 and WS_2. *Phys. Rev. B Condens. Matter Mater. Phys.* **2011**, *84* (15), 155413.